

Experimental study of multilayer adsorption on fractal surfaces in porous media

Jian Ma*

Department of Physics, Amherst College, Amherst, Massachusetts 01002

Hao Qi and Po-zen Wong

Department of Physics, University of Massachusetts, Amherst, Massachusetts 01002

(Received 19 August 1998)

We report a nitrogen adsorption isotherm study on three shale samples that have been previously characterized by small-angle neutron scattering (SANS). The scattering data establish that the pore surfaces in these porous materials are self-similar fractals over a range of length scales between 5 and 500 Å, and the fractal dimension D varies between 2.59 and 2.83. For isothermal adsorption of multilayer liquid film on fractal surfaces, the theoretical predictions are (i) the number of adsorbed molecules N increases with the vapor pressure P as $N \sim [\ln(P_0/P)]^{D-3}$ and (ii) the area of the liquid-vapor interface S_l decreases as $S_l \sim [\ln(P_0/P)]^{D-2}$. We find that fitting our data to these predictions results in D values that are significantly lower than the SANS results. More careful examination of the data reveals systematic deviations from the predicted power-law behaviors. We discuss the assumptions and approximations made in the theories that could have caused this discrepancy. [S1063-651X(99)06302-3]

PACS number(s): 68.15.+e, 68.35.Ct, 61.43.-j, 05.70.-a

I. INTRODUCTION

How gas molecules are adsorbed onto solid surfaces with increasing vapor pressure is one of the oldest questions in surface physics [1]. Porous media are often used to study adsorption phenomena for their large internal surface area [2], but the experiments do not always agree with the theories. This is commonly attributed to the fact that the classical theories of adsorption consider only uniform and planar surfaces, while in fact most porous materials have internal surfaces that are heterogeneous and irregular. In recent years, it has become widely accepted that the geometric irregularities in many materials are statistically scale invariant, i.e., they can be described as *self-similar fractals* with noninteger dimensions D between 2 and 3 [3–7]. As a result, much effort has been directed towards an understanding of adsorption on fractal surfaces [8]. However, adsorption experiments on well-characterized fractal systems are limited. The purpose of this paper is to present such a study so that the theoretical predictions can be tested.

The initial suggestion that fractal surfaces are ubiquitous in porous media came from Avnir, Farin, and Pfeifer [3]. They observed that the internal surface area of many natural materials (rocks, coals, etc.), as determined by the standard BET (Brunauer-Emmett-Teller) adsorption isotherm technique [1,2], appeared to decrease as the size of the adsorbed molecules is increased. A canonical property of fractal surfaces is that the area S decreases as a power law of the resolution of measurement l :

$$S \sim l^2(L/l)^D \sim l^{2-D}, \quad (1)$$

where L is the linear size of the surface. Using this formula to fit the data with l as the size of the adsorbed molecules,

Avnir *et al.* found that the fractal dimension D varied between 2 and 3 for different materials. However, there are several reservations about their study [9–11]: the range of length scales probed by changing molecular size is very limited, and the shape of the adsorbed molecules and their interactions with heterogeneous surface can alter the apparent area even in the absence of geometric roughness. In fact, one may question whether the BET theory should be used to determine the surface area in the first place, because it is intended for planar surfaces with uniform adsorption potentials, not for surfaces that are chemically inhomogeneous and geometrically irregular. Nevertheless, a number of later studies confirmed the ubiquitous presence of fractal surfaces in porous media. Katz and Thompson used image analysis to show that the pore-grain interfaces in sandstones are self-similar over the length scale between 0.1 and 10 μm , with D between 2.57 and 2.87 [4]. Bale and Schmidt studied lignite coal with small-angle x-ray scattering (SAXS) and found D equal to 2.56 [5]. Wong, Howard, and Lin used small-angle neutron scattering (SANS) to study sandstone and shale samples and found D between 2.55 and 2.96 over a range of 5–500 Å [6]. The qualitative picture that has emerged from these studies is that while the scaling behavior can extend over several decades of length scales, the fractal dimension D varies from system to system.

Studying adsorption of multilayer films on fractal surfaces with a single adsorbate, say, nitrogen molecules, is free of many of the complications in the original work of Avnir *et al.* [3] Chemical heterogeneity on the surface should be unimportant because the substrate becomes mostly shielded after the completion of the first monolayer. The thermodynamics of the liquidlike film and the vapor is the key consideration. The thickness of the film (z) should set the *minimum* radius of curvature of the liquid-vapor interface (r), either of which may be used as the measurement resolution l in Eq. (1). These lengths can be varied from a few angstroms to a few hundred angstroms as the vapor pressure P is in-

*Electronic address: jma@amherst.edu

creased toward the saturation value P_0 at a fixed temperature T . Fripiat *et al.* [12] and Cole *et al.* [13] extended the BET theory to fractal surfaces, but Ross *et al.* [14] found that fitting adsorption data to these theories resulted in D values that disagreed with scattering data. Pfeifer *et al.* [15] modified the Frankel-Halsey-Hill (FHH) theory which was originally intended for van der Waals adsorption on planar surfaces, but Sahouli *et al.* [16] and Ismail and Pfeifer [17] found that using their modified FHH theory to analyze adsorption data gave unphysical D values (less than 2) in some systems. The failure of these theories may be attributed to the fact that both the BET- and FHH-type models ignore the liquid-vapor surface tension, that is, the lateral interactions among the adsorbed molecules [18].

The surface tension (γ) is actually a key consideration for liquidlike film adsorbed on fractal surfaces. Since the liquid-vapor interface is curved everywhere, for a spherical meniscus with radius of curvature r , the capillary pressure ($2\gamma/r$) determines the equilibrium state of the two phases across it. The well-known Kelvin equation relates the capillary pressure to the chemical potentials of the vapor (μ) and the bulk liquid with a flat surface (μ_0):

$$\frac{2\gamma}{r} = \frac{\mu_0 - \mu}{V_L/N_A} = \frac{RT}{V_L} \ln(P_0/P), \quad (2)$$

where V_L is the molar volume of the liquid phase, N_A is Avogadro's number, and R is the universal gas constant [1,2]. As a result, more recent theories considered the growth of the liquid film as a sequence of capillary condensation in increasingly large pores as the pressure is increased. Various authors have arrived at similar predictions for the isotherm equation [19–21]. Several experiments have reported apparent power-law behaviors that seem to be consistent with the theoretical predictions, but most were not performed on systems of known fractal dimensions [16,17,22,23]. In one study on carbon black that included both adsorption isotherm and scattering experiments [24,25], the D values obtained by the two methods disagreed. However, the scattering data in this case did not cover a wide range of length scales, and it is also unclear whether the same range was probed by the isotherms. Surveying over the literature, we find only one instance where the isotherm and scattering data were claimed to agree [26], but it turned out to be a misinterpretation of the scattering data [27,28]. It is fair to say that the theoretical predictions in Refs. [18–21] have not been fully tested.

In this paper, we report an adsorption isotherm experiment on several shale samples for which the surface fractal dimensions D are known from previous SANS experiments. The isotherm data are taken to cover the same range of length scales as that probed by SANS. Care was taken to ensure that the thermal equilibrium was reached for every data point, and desorption data were taken to explicitly identify the capillary condensation regime. Our results show that although the adsorption data exhibit approximate power-law behavior, the D values obtained using the existing theories are consistently lower than the SANS results. There are also systematic deviations from the simple power-law behaviors predicted by the theories. Some of these may be attributed to structural changes in the adsorbed film with the film thickness, that is to say that the film does not have a constant

density or surface tension like a bulk liquid. More importantly, we believe some of the implicit assumptions and approximations made in the theories may not be justified. Our main conclusion is that while the fractal nature of the pore surface affects the adsorption behavior, the D value cannot be determined from the adsorption isotherms using the current theoretical methods.

The organization of this paper is as follows. In Sec. II we give a brief review of the theoretical background and the expressions used to analyze the adsorption data. In Sec. III we describe the experimental method and the sample properties, including the SANS data. In particular, we show that the two techniques probe the same length scales in the samples we have chosen. We then present the isotherm data and analyses in Sec. IV, and compare the results given by the two techniques. In Sec. V, we discuss our findings.

II. THEORETICAL BACKGROUND

An adsorption isotherm experiment measures the amount of gas adsorbed on a substrate as a function of the equilibrium vapor pressure P at a fixed temperature T . The surface area (S) of the substrate is determined by the number of adsorbed molecules (N_m) required to cover the surface with a monolayer and the cross-sectional area (σ_m) of the molecule. For a fractal surface of linear size L and dimension D , if the adsorbed molecules are of size l , the combination of two basic relationships, $N_m \sim (L/l)^D$ and $\sigma_m \sim l^2$, yields Eq. (1). It should be noted that in any real system, the power-law behavior extends only over a finite range of length scales, say, from l_- to l_+ . The lower limit l_- may be as small as a few angstroms, while the upper limit l_+ can be as large as the pore radius. A smooth surface satisfies Eq. (1) with $D = 2$, whereas a fractal surface can have $2 < D < 3$. In a multilayer adsorbed film, the thickness of the film z shields the small features on the surface. The *minimum* radius of curvature r of the liquid-vapor interface is usually *assumed* to be proportional to z (see Sec. V, however), hence either r or z may serve as the measuring yardstick l . According to Eq. (1), the volume of the adsorbed film is

$$V \approx zS \propto z^3 (L/z)^D \propto z^{3-D} \propto r^{3-D}. \quad (3)$$

Further assuming that the surface tension and the density of the film do not change with the film thickness, it follows from Eq. (2) that the number of adsorbed molecules in the film is given by

$$N = N_0 [\ln(P_0/P)]^{D-3}, \quad (4)$$

where N_0 is a characteristic constant. This equation is commonly referred to as the *fractal* FHH equation. Kardar and Indekeu [18] and Cole and Pfeifer [8] came to this conclusion by the simple scaling argument given above. Other authors modeled the fractal surface as a collection of pores obeying a power-law pore size distribution $g(r)$, and considered the adsorption in each pore as the pressure is increased. We note that if the number density of pores of size r is given by $g(r) \sim r^{-(1+D)}$, the surface area measured with a resolution l is

$$S \sim \int_l r^2 g(r) dr = \int_l r^{1-D} dr \sim l^{2-D} \quad (5)$$

consistent with Eq. (1). Avinir and Jaroniec [19] assumed that the adsorption in each pore obeys the Dubinin-Radushkevich (DR) isotherm which implicitly has $r \propto [\ln(P_0/P)]^{-1}$, similar to Eq. (2). Yin [20] considered the sequential capillary condensation in pores from small to large, according to Eq. (2), as the pressure is increased. In both cases, the isotherm equation is obtained by integrating the single pore filling over the size distribution $g(r)$, which results in Eq. (4).

It should be noted that the above theories ignore the substrate potential and focus only on the liquid-vapor equilibrium. Pfeifer and Cole considered the relative strength of the substrate potential and the surface tension. They estimated that capillary condensation would occur when the film thickness z exceeds 10 \AA . Below this thickness, they argued that the substrate potential would dominate and the exponent in Eq. (4) should be $(D-3)/3$, due to the long-range $1/z^3$ van der Waals potential (which is experienced by an adsorbed molecule near the surface of a semi-infinite solid). In practice, however, the range of thickness between one monolayer and 10 \AA is too small for the scaling behavior to be observed. This implies that in analyzing data in the thick-film regime, an additional constant term should be included in Eq. (4) to represent the amount adsorbed before capillary condensation begins, that is,

$$N = N_0 [\ln(P_0/P)]^{D-3} + N_B. \quad (6)$$

A somewhat different line of reasoning based on thermodynamics was adopted by Neimark [21]. He argued that the area of the liquid-vapor interface S should obey Eq. (1) with its minimum radius of curvature r as the measuring yardstick. The increase in film thickness due to condensation raises r and, therefore, results in a smaller area S . Since the increase in bulk chemical potential is compensated by the reduction in interfacial free energy, i.e., $\gamma dS + (\mu_0 - \mu) dN = 0$, integrating from an initial film thickness in the fractal regime to the upper cutoff gives

$$-\int_S^{S_+} dS = S - S_+ = \frac{k_B T}{\gamma} \int_N^{N_+} \ln(P_0/P) dN. \quad (7)$$

Using Eqs. (1) and (2), the integral on the right-hand side should obey

$$S_I \equiv \frac{k_B T}{\gamma} \int_N^{N_+} \ln(P_0/P) dN = S_0 [\ln(P_0/P)]^{D-2} - S_B, \quad (8)$$

where S_0 and S_B are empirical constants. This prediction can be tested by numerically integrating the isotherm data to obtain S_I and performing a least-squares fit. The uncertainty in the choice of the integral's upper limit is unimportant because it affects only the background constant S_B but not the power-law form. This approach is commonly referred to as the *thermodynamic method*.

Although the predictions of Eqs. (6) and (8) appear to be quite different, they both follow directly from Eqs. (1)–(3)

TABLE I. Basic properties of the samples.

Sample	H2	H4	H8
Diameter (cm)	1.994(2)	1.999(2)	1.994(1)
Thickness (cm)	0.315	0.310	0.307
Sample volume (cm ³)	0.984	0.973	0.959
Sample weight (g)	2.3457	2.2070	2.2210
Bulk density ρ (g/cm ³)	2.3846	2.2684	2.3167
Porosity $\phi = 1 - \rho/\rho_g^a$	8.3%	12.8%	10.9%
Mean pore diameter (Å) ^b	110	165	172
Breakthrough diameter (Å) ^b	660	490	700
D from SANS	2.83	2.75	2.59

^aCalculated based on an assumed grain density $\rho_g = 2.60 \text{ g/cm}^3$.

^bFrom mercury injection analyses that assumed cylindrical pores.

[29], because the integral in Eq. (8) can be rewritten as $\int r^{-1} d(r^{3-D}) \propto r^{2-D}$. The main difference between Eqs. (6) and (8) is in the additive constant, which is important in analyzing the experimental data. That is, N_B in Eq. (6) represents the molecules adsorbed on the surface before capillary condensation initiates, whereas S_B in Eq. (8) is the area of the liquid-vapor interface present when all the pores in the fractal regime are filled. In performing least-squares fits of the data, the fitting parameters are inevitably correlated and these additive constants can affect the apparent exponent. In Sec. IV, we present analyses using both equations so that we can assess the importance of this systematic error.

III. SAMPLE PROPERTIES AND EXPERIMENTAL METHOD

Three samples of Frio shale, designated as H2, H4, and H8, are chosen for this study. Table I lists their basic properties. Each sample is in the shape of a disk, approximately 2 cm in diameter and 0.31 cm in thickness. The bulk densities of these samples are about 2.3 g/cm^3 . Since the grain densities of common clay minerals and sands are approximately 2.6 g/cm^3 [30], the estimated porosities of these samples are in the neighborhood of 10%. Based on mercury injection analyses, which assume cylindrical pores, the pore diameters are below 1000 \AA in these samples, with mean values varying between 100 and 200 \AA .

SANS experiments had been previously performed on the same samples and D was found to be 2.83, 2.75, and 2.59 for H2, H4, and H8, respectively. The SANS experimental details are described in Ref. [6]. We note here only that the scattering cross section per unit volume, or the intensity I , as a function of the wave-vector transfer q falls off as a power-law [6,27],

$$I(q) = \frac{A}{q^{6-D}} + B, \quad (9)$$

where A is proportional to the internal surface area of the sample and the constant B comes from the uncorrelated disorder in the system. Figure 1 shows the SANS data and the fits to Eq. (9) that resulted in the above D values. We note that the H2 and H4 data cover about two decades in q ($0.002 < q < 0.2 \text{ \AA}^{-1}$) and were taken on the same samples as those used for the present study. The H8 data span only

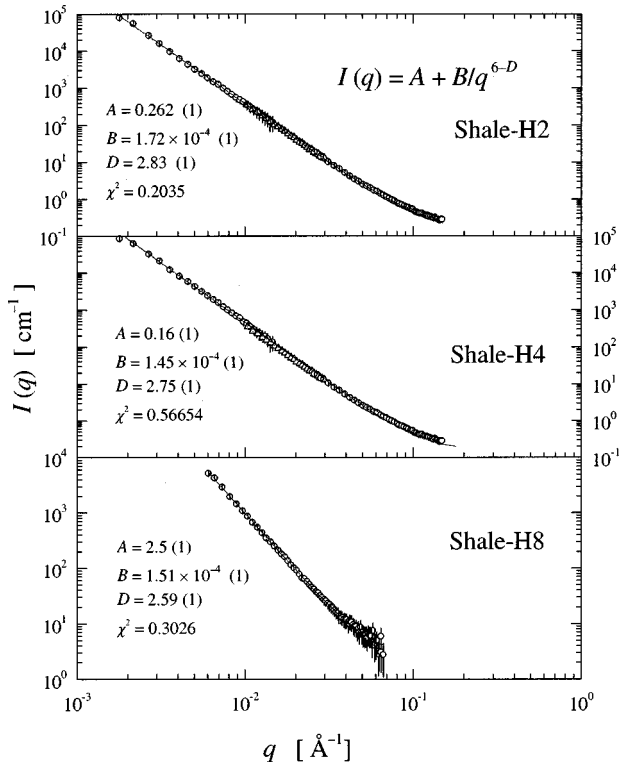


FIG. 1. Small-angle neutron-scattering data of the shale samples are well described by Eq. (9).

one decade in q and were taken on a 1-cm-thick sample that was subsequently ground to a 0.3-cm thickness and used in this work. Although some systematic deviations from the fits can be detected, especially near the two ends of the scale, the middle range ($0.005 < q < 0.05 \text{ \AA}^{-1}$) is well described by the power-law term in Eq. (9) and insensitive to the background constant B . This range corresponds to length scales ($l \sim 1/q$) between 20 and 200 \AA which, as well shall see, falls into the capillary condensation regime where Eqs. (6) and (8) should be applicable. We note that although statistical errors in the D values given by the fits are within 0.01, the actual uncertainties may be as large as 0.05 when the ranges of the fits are varied. Nevertheless, the differences in D values among the three samples are large enough that we believe they are not experimental artifacts.

The properties of the three samples obtained from our isotherm data are listed in Table II. In particular, we note that all three samples have specific areas of approximately $10 \text{ m}^2/\text{g}$, which are an order of magnitude larger than those of

TABLE II. Sample properties obtained from isotherm data.

Sample	H2	H4	H8
P_0 (torr)	133.2(1)	133.6(1)	133.4(1)
Temperature (K)	65.121	65.138	65.131
V_{full} (cm^3 -STP)	74.5	89	78
Porosity	11.0%	13.3%	11.8%
V_{40} (V_{ad} adsorbed at 40 torr)	11.2	6.5	5.8
BET V_m (cm^3 -STP)	7.5	4.2	3.8
Total BET area S_{BET} (m^2)	31.4	17.6	15.9
BET specific area (m^2/g)	13.4	8.0	7.2

common sandstones and limestones. This is important because the sample must have a surface area that is much larger than that of the apparatus. We note that the cross-sectional area of a nitrogen molecule is approximately 0.156 nm^2 at 65 K [31]. A monolayer covering an area of 20 m^2 requires about 1.19×10^{20} molecules, which corresponds to an STP gas volume (V_m) of 4.4 cm^3 . In contrast, the total pore volume of a 10% porosity sample is about 0.094 cm^3 and filling it with liquid nitrogen at 65 K (density $\rho = 0.86 \text{ g/cm}^3$) requires an STP volume of 64.8 cm^3 (or 0.081 g). This volume is designated as V_{full} , whose values for the three samples are listed in Table II. Based on the ratio V_{full}/V_m , we expect that the power-law behavior in Eq. (6) is limited to about one decade in N . It is also important to point out that the mean pore diameters of these samples, as determined by mercury injection and listed in Table I, are less than 200 \AA . Hence the upper cutoff of the fractal behavior should be at a comparable length scale. Since the lower cutoff of the capillary condensation regime is expected to be above 10 \AA , the length scales probed by the adsorption isotherm are well matched to that probed by the SANS experiment.

Before measuring the nitrogen adsorption isotherm, the foreign molecules adsorbed in the sample over its lifetime have to be removed. This was achieved by first placing the sample in a quartz tube and having it pumped on continuously for several days using a standard two-stage pumping station. After this precleaning, the sample was quickly transferred to a cylindrical copper cell used for the adsorption experiment. The inner diameter of the cell body (2.03 cm) was made to fit the sample snugly but the height (0.76 cm) was chosen to accommodate a range of sample thickness. In order to enhance temperature stability, the lid of the cell was made to have a large thermal mass: a 180-g copper disk about 6.35 cm in diameter and 0.635 cm in thickness. (The cell body and the sample together weigh about 30 g) A 51- μm -diam indium wire was used to make the vacuum seal between the cell body and the lid. A stainless-steel capillary of inner diameter 0.81 mm was soldered to the lid and connected the cell to the gas-handling system. The entire cell assembly was mounted on a CTI closed cycle refrigerator which can cool down to 10 K. A heater wire (80- μm -diam manganin with a resistance of about 58 Ω) was wound around the lid to vary the sample temperature between 10 K and room temperature. A resistance thermometer (a Lake-Shore Cernox CX1070 sensor) was attached to the top of the lid, and a Quantum Design 1802 resistance bridge was used to detect and control the temperature. We were able to achieve a stability of about $\pm 3 \text{ mK}$.

The temperature of the experiment, 65 K, was chosen for two reasons. First, it is above the triple point of nitrogen (63.14 K), so that the equilibration is between a liquidlike *wetting* film and the vapor [31]. Second, because the surface tension γ increases with decreasing temperature T , according to Eq. (2), by keeping T low and γ large we can probe larger length scales r without approaching the saturation pressure too closely. We note that because r diverges as $P \rightarrow P_0$, the conversion from P to r becomes unreliable near P_0 , which ultimately limits the length scales that could be reliably probed by the isotherms. Based on the known values of surface tension for bulk liquid nitrogen at 70, 80, and 90 K [32],

we estimate $\gamma \approx 12$ dyn/cm for nitrogen at 65 K. Using Eq. (2) with $V_L = 32.56$ cm³/mol [32], the conversion relation is

$$r = \frac{2\gamma V_L}{RT \ln(P_0/P)} \approx \frac{14.5 \text{ \AA}}{\ln(P_0/P)}, \quad (10)$$

where P_0 is approximately 133 torr at 65 K. Using Eq. (10), the range of r probed by SANS, 5–500 Å, corresponds to $0.055 < P/P_0 < 0.97$, and the middle part of this range, 15–150 Å, corresponds to $0.38 < P/P_0 < 0.91$. Hence the match between the two types of experiments is nearly ideal. Our pressure measurements were made with a MKS capacitance gauge which has a resolution of 0.01 torr and covers a range of 0–1000 torr.

The isotherm measurements were made with a gas-handling system situated at room temperature (295 ± 1 K). It has a fixed dosing volume which holds nitrogen gas at an initial pressure P_i and is connected to the sample cell through a valve. When the valve is opened briefly, a dose of gas is let into the sample cell and the pressure in the dosing volume decreases to a final value P_f . From the reduction in pressure ($P_f - P_i$) and the ideal gas law, we can deduce the number of molecules N_{tot} entering the sample cell. In practice, we use the gas volume V_{tot} (expressed in units of cm³-STP) as a measure of N_{tot} . (They are related by $N_{\text{tot}}/N_A = V_{\text{tot}}/22.4$ liters.) A nitrogen gas supply is used to recharge the dosing volume when it is near depletion. The volume of the dosing container is 33.0(5) cm³, where the uncertainty is due to the inaccuracy in estimating the volume in the connecting valves. This error is unimportant because it only changes N_{tot} by a constant multiplicative factor. However, room-temperature variations (~ 1 K) during the course of the experiment affect the pressure reading in the dosing container and consequently cause the dosage to fluctuate by about 0.3%. In addition, we note that some of the gas molecules that enter the cell get adsorbed on the container wall (about 11 cm² in area), and some fill the space surrounding the sample and in the connecting capillary (total about 2.3 cm³ in volume). The former is negligible compared with the amount adsorbed inside the sample, and the latter has been subtracted from V_{tot} to obtain the actual amount adsorbed inside the sample (V_{ad}). Taking into account all sources of errors, we estimate that the total error in V_{ad} is less than 1%. The worst case occurs at the low pressure end where the accuracy of the pressure gauge and the vapor background correction are more important, but that is not the range for fractal analyses.

An important feature of our apparatus is that it allows ample time for the sample to reach thermal equilibrium after each incremental dose of gas. While commercial apparatus built to determine BET area can finish an adsorption-desorption cycle in less than an hour, each of our adsorption steps took about two hours. A computer is used to monitor the pressure change with time after each dose. When there is no change within the reading resolution (0.01 torr) over 10 min we consider equilibrium is reached. We shall also point out that on desorption near 40 torr, the lower limit of the capillary condensation regime, the equilibration time was found to be as long as eight hours. Altogether, a complete adsorption-desorption cycle typically took more than one week of continuous data acquisition.

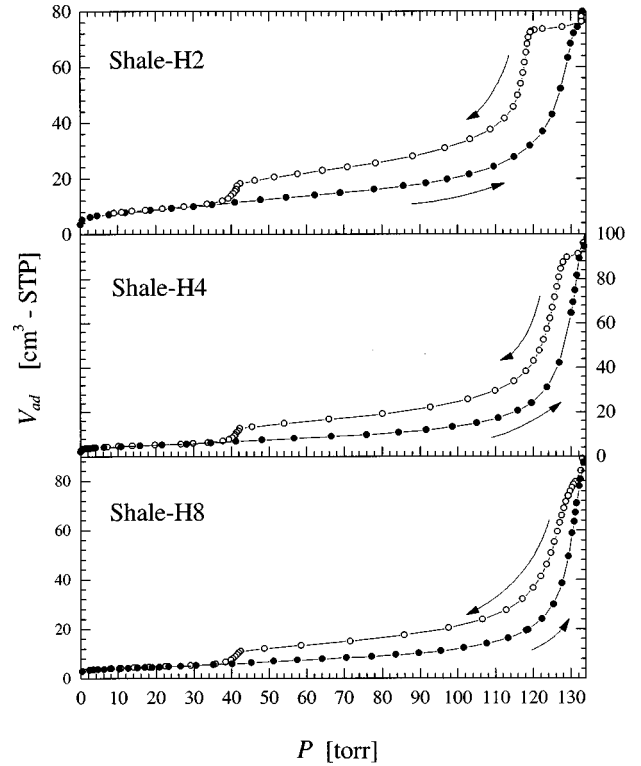


FIG. 2. Adsorption-desorption isotherms of nitrogen in three shale samples at 65 K. Bulk condensation occurs at about 133 torr. Capillary condensation begins at about 40 torr for all three samples.

When the precleaned sample was first transferred to the apparatus, the system was pumped on through the gas-handling system. The outgassing rate was monitored periodically by letting the sample out-gas to the dosing volume without pumping. Only when the pressure rise was less than 0.02 torr per hour did we begin cooling down the sample for isotherm measurements. To ensure that the data were reproducible, we took data on each sample with at least two adsorption-desorption cycles. This also turned out to be convenient in that the first run usually mapped out the overall features of the isotherm and the second filled in additional data points where needed.

IV. RESULTS AND ANALYSES

Figure 2 shows the nitrogen adsorption-desorption isotherms for the three samples at 65 K where the adsorbed amount V_{ad} is plotted as a function of pressure P . In each case, we observe an extended hysteresis loop which is the signature of capillary condensation. At the low pressure end, hysteresis sets in around 40 torr. At the upper end, there is a vertical rise just above 133 torr that marks the onset of bulk condensation of nitrogen, and hence the saturation pressure P_0 . Using Eq. (10), we find that 40 torr corresponds to a minimum length scale $r_{\text{min}} \approx 12$ Å, consistent with Cole and Pfeifer's estimate of film thickness $z \approx 10$ Å [8].

Figure 3 shows the details of the isotherms near saturation. We note that P_0 for the three samples differ slightly, about ± 0.2 torr. This is due to the fact that the temperature of the sample cell could be reliably set only within ± 0.01 K. The precise values of P_0 are listed in Table II. Just below P_0 , near 132 torr as marked by an arrow, the adsorption and

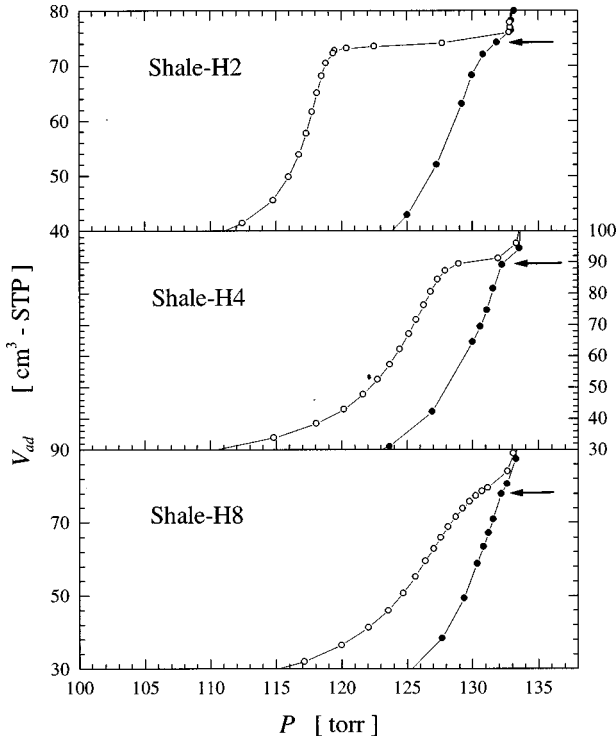


FIG. 3. Close-up view of the isotherm data near bulk saturation. The arrows mark the points where the adsorption and desorption data begin to diverge significantly, which signal the end of capillary condensation. This occurs at about 132 torr for all three samples. The total amount adsorbed at this point (V_{full}) is used to estimate the porosity of the samples.

desorption data begin to diverge. We use this feature as an indication of the end of the capillary condensation regime. Although small differences between the adsorption and desorption data persist above this pressure, they could be due to condensation on the outer surface of the sample and not in its interior pores. Assuming that all the interior pores are filled up to 132 torr, we determine V_{full} for each sample. From the density of liquid nitrogen at 65 K (0.86 g/cm^3) and the sample dimensions, we find that the sample porosity ϕ is between 11% and 13%. The values of ϕ for the three samples are given in Table II, and they are consistent with the values listed in Table I. According to Eq. (10), 132 torr corresponds to a maximum length scale $r_{\text{max}} > 1000 \text{ \AA}$ (the exact value is sensitive to small variations in P_0). Thus the range of r probed by the capillary condensation regime is roughly between 12 and 1000 \AA . This is consistent with the mercury injection data which give *mean* pore diameters in the range of $100\text{--}200 \text{ \AA}$ and breakthrough diameters in the range of $500\text{--}800 \text{ \AA}$ (see Table I). Due to the form of Eq. (10), the conversion from P to r is highly sensitive to the choice of P_0 near saturation. Since the maximum length scale ($\sim 1/q$) probed by SANS is only 500 \AA and equating it with r in Eq. (10) gives $P = 129 \text{ torr}$, we limit our analyses to data below this pressure. We can see from Fig. 3 that 129 torr is safely inside the capillary condensation regime and the small change in the choice of P_0 is inconsequential to the calculation of r .

For the data below the capillary condensation region (i.e., $P < 40 \text{ torr}$ in Fig. 2), we first performed the standard BET analyses using the equation

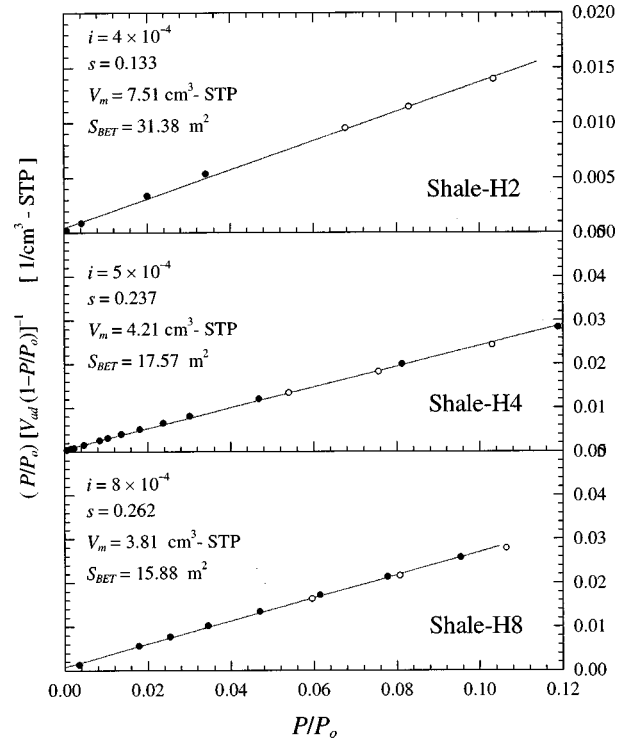


FIG. 4. BET plots of the low pressure data (from both adsorption and desorption isotherms) for the three samples. The surface area is determined from the slope s and the intercept i of the fit according to Eq. (12).

$$\frac{P/P_0}{V_{\text{ad}}(1-P/P_0)} = \frac{1}{V_m c} + \frac{1-c}{V_m c} (P/P_0), \quad (11)$$

where c is the BET constant and V_m is the monolayer capacity expressed in $\text{cm}^3\text{-STP}$ (that is, $V_m/0.0224 \text{ m}^3 = N_m/N_A$). In Fig. 4 we show plots of the left-hand side of Eq. (11) versus P/P_0 for all three samples, using both adsorption and desorption data in the range $P/P_0 < 0.12$ (or $P < 16 \text{ torr}$). That the points fall on a straight line indicates that Eq. (11) works well, despite the fact that the assumptions in the BET model are not expected to hold for these highly heterogeneous samples. The slope of the line $s = (1-c)/V_m c$ and the y intercept $i = 1/V_m c$ are used to compute the monolayer capacity: $V_m = 1/(s+i)$. In practice, we find $i \ll s$, hence $V_m \approx 1/s$. The BET surface area is given by

$$S_{\text{BET}} = \frac{\sigma_m N_A V_m}{0.0224 \text{ m}^3} = \frac{4.18 \text{ m}^2}{i+s}, \quad (12)$$

where σ_m is the effective area of a single nitrogen molecule. (At 77 K, σ_m for nitrogen is usually taken to be 16.2 \AA^2 based on the liquid density of 0.81 g/cm^3 , which is supported by the experimental observations on a variety of surfaces [2]. We use $\sigma_m \approx 15.6 \text{ \AA}^2$ at 65 K based on the increased density of 0.86 g/cm^3 [31].) The values of V_m and S_{BET} for each sample are listed in Table II. We should note that the V_m and S_{BET} are only weakly sensitive to the pressure range we choose to perform the BET analyses. For example, even using data up to $P/P_0 \approx 0.4$ (or $P \approx 53 \text{ torr}$), which extends into the capillary condensation regime, V_m and S_{BET} increase only by 10–15%, but small systematic deviations from lin-

earity can also be seen in plots like those in Fig. 4. While it may be tempting to improve the fits of the low-pressure data by using the fractal BET model [12,13] or the fractal van der Waals model [15], which ignore surface tension effects, it would be misleading to do so. We list in Table II the amount adsorbed at 40 torr (V_{40}) for each sample and note that they are only about 50% larger than V_m . This implies that capillary condensation begins when the adsorbed film is no more than two layers thick on average, or $z < 8 \text{ \AA}$. The fractal models in Refs. [12,13,15] are intended to describe the region between a monolayer and the onset of capillary condensation. For the present case, this would mean between one and two layers. Clearly, scaling analysis over such a narrow range would not be meaningful. Furthermore, it is useful to note that $P=40$ torr in Eq. (10) gives $r \approx 12 \text{ \AA} > z$. With the usual assumption that $r \propto z$, we expect the film thickness to be always less than the Kelvin radius computed from Eq. (10). A proper fractal analysis should use only the adsorption branch of the isotherm above 40 torr. The reason that the desorption branch is not applicable is that on desorption the pores in the interior of the sample that satisfy Eq. (10) cannot empty until those on the outer part have emptied, so that they can have access to the surrounding vapor [33]. This accessibility is not an issue on adsorption.

Fractal analyses found in the literature [16,17,22–24] are based on fitting adsorption data to Eqs. (6) and (8), but they often ignore the background constants. Typically a linear fit of the data on log-log scales is used to find a slope, from which the fractal dimension D is obtained. In Figs. 5 and 6, we show the results of such analyses. Figure 5 consists of plots of $\log_{10}(V_{ad}/V_{full})$ versus $\log_{10}(r)$ for the adsorption data, where r is calculated from the pressure P using Eq. (10). The data appear to fit a straight line over about two decades in r . The range of the fit is indicated by the arrows in each plot, approximately between 4 and 500 \AA . Based on Eq. (6) without the constant term N_B , the slope of the line should be $3 - D$. We find that the D values so obtained fall in the range 2.43–2.54, somewhat lower than the values obtained by SANS over the same range of length scales. Similar analyses using Eq. (8) without the constant term S_B do not fare much better. The integral for S_I in Eq. (8) was computed numerically from the adsorption data using the standard trapezoidal rule. Figure 6 shows plots of $\log_{10}(S_I)$ versus $\log_{10}(r)$ for the three samples. Similar to Fig. 5, the data appear to follow a straight line over nearly two decades in r . If the slope of the line were to be $(2 - D)$, the D values would be between 2.50 and 2.63, slightly higher than those obtained from Fig. 5, but still lower than the SANS results.

Table III tabulates the D values obtained from Figs. 5 and 6. We note that they are consistently lower than the SANS results for all three samples. The disagreement is not surprising since Eqs. (6) and (8) should not be applied over such a wide range of length scales and the additive constants should be included to represent contributions outside the fractal regime. In both Figs. 5 and 6, we divide each plot into four quadrants with a horizontal dashed line corresponding to the BET monolayer coverage and a vertical dotted line at $r = 12 \text{ \AA}$ marking the onset of capillary condensation. It should be clear that Eqs. (6) and (8) are applicable only to the data points that are to the right of the vertical lines. Careful examination of the data in Figs. 5 and 6 reveals that

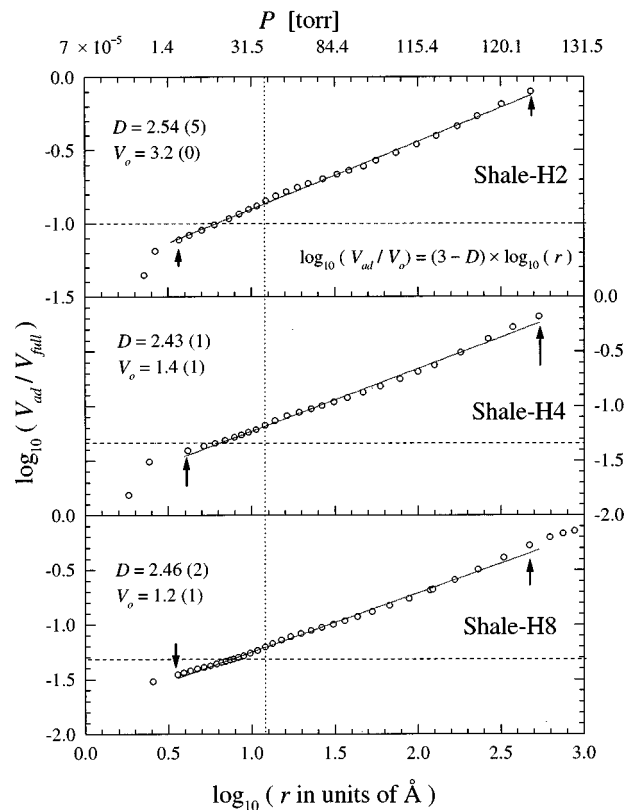


FIG. 5. $\log_{10}(V_{ad}/V_{full})$ vs $\log_{10}(r)$ for the three samples using the adsorption isotherm data in Fig. 2. The plots appear to be linear over two decades in r . According to Eq. (6), the slope is $3 - D$. The arrows indicate the range of data used in the linear regression. The horizontal dashed line corresponds to the BET monolayer coverage and the vertical dotted line marks the pressure (40 torr) at which capillary condensation begins. Note that Eq. (6) is applicable only to the data to the right of the vertical dotted line.

they display the same pattern of systematic deviations from the straight line. Each plot in Fig. 5 exhibits a shoulder just to the right of the vertical line and the corresponding plot in Fig. 6 shows a dip at the same place. The slope of each plot in Figs. 5 and 6 steepens with increasing r beyond this point ($r \approx 20 \text{ \AA}$), which is consistent with a positive background term in Eq. (6) and a negative one in Eq. (8).

Figures 7 and 8 show the analyses using only the adsorption data in the capillary condensation regime. The solid lines represent the results of nonlinear least-squares fits to Eqs. (6) and (8). The lower limits of all the fits are chosen to be about 20 \AA to be safely above the 12 \AA threshold. The upper limits of the fits vary between 300 and 500 \AA . With an extra fitting parameter and a narrower range, the quality of the fits is improved compared to that in Figs. 5 and 6. However, the D values so obtained are even lower, in the range of 2.2–2.4 as given in Table III, making them unmistakably lower than the SANS results. We note that H2 has the highest D value in every analysis. H4 and H8 have nearly the same D values from the isotherms, but differ in their SANS results. The latter may be due to the fact that the SANS data on H8 were taken on a thicker sample and over a smaller range of q , thus not directly comparable. It is interesting to observe that the horizontal dashed lines in Fig. 6 (or Fig. 8) intersect the data points at r values (or pressures) slightly

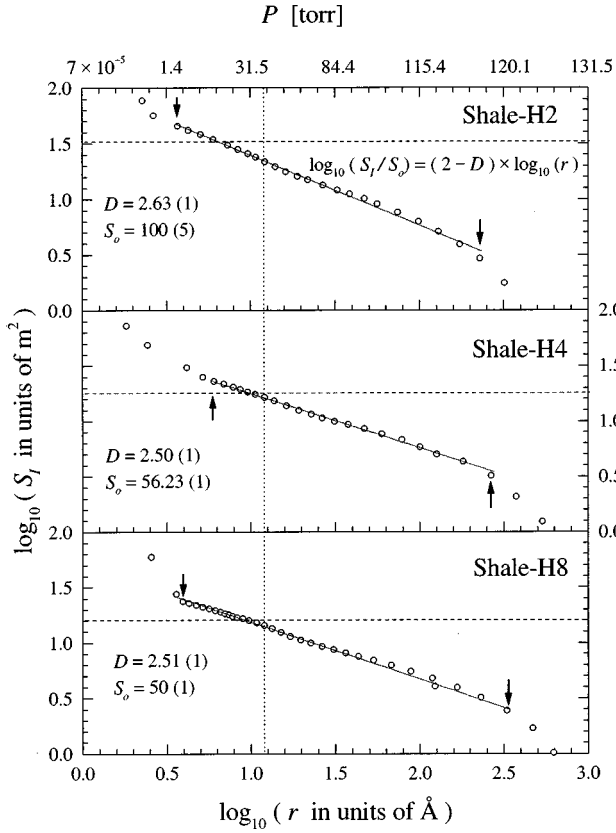


FIG. 6. $\log_{10}(S_f)$ vs $\log_{10}(r)$ for the three samples using the adsorption isotherm data in Fig. 2. The plots appear to be linear over about two decades in r . According to Eq. (8), the slope is $2 - D$. The arrows indicate the range of data used in the linear regression. The dashed and dotted lines have the same meanings as those in Fig. 5. Note that Eq. (8) is applicable only to the data to the right of the vertical dotted line.

higher than those in Fig. 5 (or Fig. 7). This shows that although Eqs. (6) and (8) are mathematically related, they can give somewhat different results in data analyses due to systematic errors. The constant N_B in Eq. (6) accounts for the amount adsorbed at the lower end of the capillary condensation regime, while S_B in Eq. (8) accounts for the liquid-vapor interface present at the upper end. The inclusion of these fitting parameters inevitably affects the other parameters in the fit. The difference in D values obtained from the two types of fits is a useful estimate of the systematic error. From the values listed in Table III, this difference is about 0.1, which is much larger than the errors of the individual fits. However, even allowing for larger error bars, we still cannot reconcile the isotherm findings with the SANS results. In the

TABLE III. Summary of D values obtained from SANS and isotherm data.

Sample	H2	H4	H8
D from SANS	2.83(1)	2.75(1)	2.59(1)
D from Fig. 5	2.54(5)	2.43(1)	2.46(2)
D from Fig. 6	2.63(1)	2.50(1)	2.50(1)
D from Fig. 7	2.39(1)	2.24(1)	2.20(1)
D from Fig. 8	2.34(2)	2.31(3)	2.31(5)

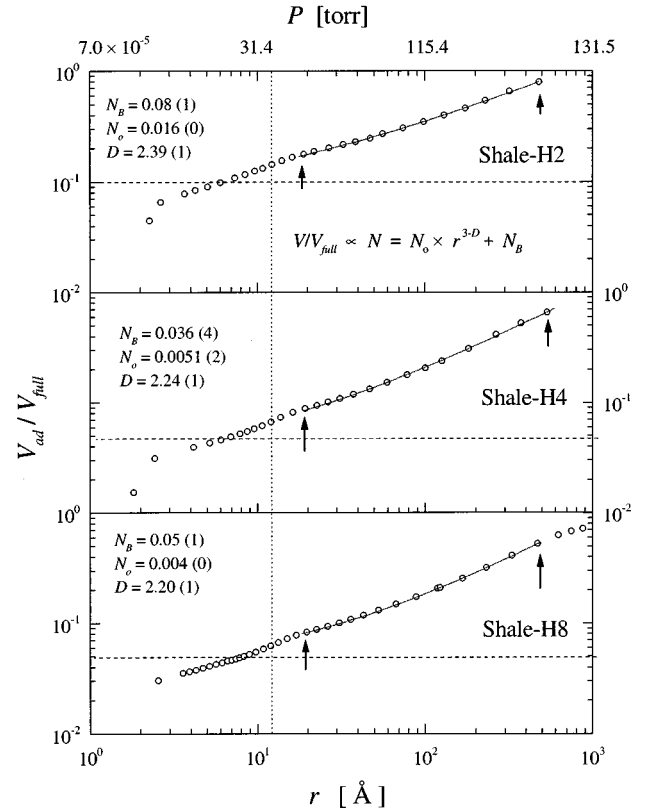


FIG. 7. Nonlinear least-squares fits of V_{ad}/V_{full} vs r using Eq. (6) in the capillary condensation region result in fractal dimensions lower than those obtained from Fig. 5. The arrows and the dashed and dotted lines have the same meanings as those in Fig. 5.

next section, we discuss the possible reasons for this discrepancy.

V. DISCUSSION AND CONCLUSIONS

From the results presented in the preceding section, it is clear that although the adsorption isotherm data exhibit apparent power-law behavior, the fractal dimensions obtained from either Eq. (6) or Eq. (8) are consistently lower than the SANS results for all three samples. This is the case regardless of how the data are analyzed. The fact that the more stringent analyses in Figs. 7 and 8 yield a larger disagreement between the two types of experiments only reinforces this conclusion. We consider here the possible reasons for this finding.

The most obvious shortcoming of the adsorption analyses has to do with using the Kelvin equation [Eq. (2)] to relate the minimum radius of curvature r to the pressure P . This is actually unphysical because it implies that the substrate geometry is irrelevant while, in fact, it is the substrate geometry that causes the local curvatures of the liquid-vapor interface to vary in the first place. Clearly, the substrate potential should not be ignored even for films that are considered to be *thick*. In other words, neglecting the substrate potential can only be justified in the limit that the film is so thick that the adsorption data offer no information about the underlying substrate geometry, which is clearly not what we are interested in. To illustrate this point more explicitly, we may consider capillary condensation inside a spherical pore.

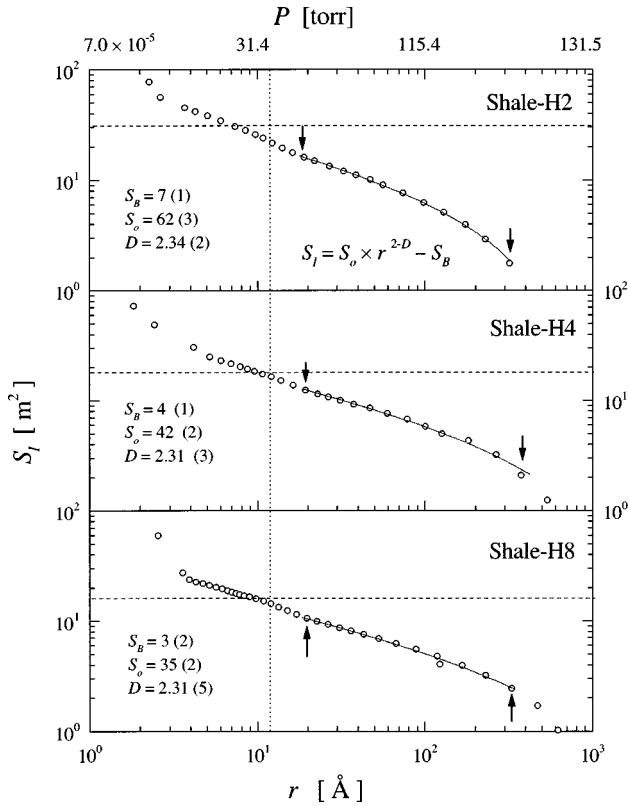


FIG. 8. Nonlinear least-squares fits of S_l vs r using Eq. (8) in the capillary condensation region result in fractal dimensions lower than those found in Fig. 6. The arrows and the dashed and dotted lines have the same meanings as those in Fig. 5.

Suppose that the pore radius is R and the radius of curvature of the meniscus is r , then the film thickness

$$z = R - r. \quad (13)$$

For a molecule of volume a^3 , in the limit of $a \ll z \ll R$, the van der Waals attraction to the pore wall is proportional to $1/z^3$. Following Cohen *et al.*'s work on cylindrical pores [34], we can write

$$\frac{\alpha a^3}{z^3} + \frac{2\gamma a^3}{r} = \Delta\mu = k_B T \ln\left(\frac{P_0}{P}\right), \quad (14)$$

where α is a constant. Equation (2) is valid if the adsorbed film is thick enough, such that the $1/z^3$ term is small and the entire film has only one radius of curvature. On a rough surface, the radius of curvature of the film might vary because the substrate potential is different everywhere and may not be of the simple $1/z^3$ form. As discussed in Sec. IV, at 40 torr where capillary condensation begins, the Kelvin radius is 12 Å and the amount adsorbed corresponds to only 1.5 BET monolayers ($V_{40}/V_m \approx 1.5$ in Table II). Thus, not only are the assumptions in the Kelvin equation unjustified, even Eq. (14) may not be a good approximation, for the pore may not be spherical and the requirement for $a \ll z \ll R$ may not be met. Nevertheless, Eq. (14) allows us to see explicitly the kind of error that can result from using the Kelvin equation to compute r in the analyses. It should be clear that with the right-hand side (RHS) fixed, including any attractive substrate potential on the left-hand side (LHS) implies a smaller

($1/r$) term. This would result in r values that are larger than those computed from Eq. (10). Since the potential is stronger and the correction to r larger at short length scales, this would result in steeper slopes in all the plots in Figs. 5–8. However, steeper slopes mean smaller D values in Figs. 5 and 7 and larger D values in Figs. 6 and 8. This apparent contradiction may be resolved by considering additional corrections due to the changes in density and surface tension of the liquidlike film with increasing thickness. We note that Ref. [2] cited calculations suggesting that the liquid-vapor surface tension γ increases by as much as 50% as the radius of curvature r is decreased from 100 to 10 Å, with a larger percentage correction at smaller r . This affects both the calculation of r in Eq. (14) and that of S_l in Eq. (8). Furthermore, the presence of the substrate potential implies that the molecular volume a^3 (density) is smaller (larger) for thinner films. How all these factors combine to change the conversion from P to r in Eq. (10) is unclear. It is fair to say that the changes in liquid properties in small pores should preclude us from using Eqs. (6) and (8) to determine the fractal dimension. In fact, the difference between the isotherm and SANS results may be exploited to understand how liquid properties are altered inside small pores.

Putting the details of liquid properties in small pores aside, a more fundamental problem has to do with the different ways by which the isotherms and the SANS probe the pore geometry. At a crude level, both techniques rely on the scaling behavior of the volume of a boundary layer that lines the pore surface with thickness z , i.e., Eq. (3), but in details they are different. The scattering function in Eq. (9) comes directly from the Fourier transform of Eq. (3) [27], so the interpretation of the data is relatively unambiguous. Still, deviations from the asymptotic $1/q^{6-D}$ behavior can occur because the range of scaling is finite and short-range correlations may exist. In the adsorption experiment, however, the liquid-vapor interface is not at a constant distance z from the surface; instead, it is smoothed by the surface tension effects and characterized by a constant chemical potential. Therefore, strictly speaking, *the volume occupied by the film is not identical to that probed by SANS*. Substituting the minimum radius of curvature r for z in Eq. (3) presumes that the two lengths are proportional to each other, and the difference in the boundary layer volume is unimportant. While these assumptions may seem intuitively reasonable they are by no means obvious or proven. It is actually not difficult to give a counterexample. Specifically, let us consider the case in which the fractal surface is represented by a power-law distribution of independent spheres with $g(r) \sim r^{-(1+D)}$ and the conditions for Eq. (14) are satisfied. In each sphere, Eq. (13) shows that an increase in the film thickness results in a decrease in the radius of curvature, thus the condition that $r \propto z$ is not satisfied. Substituting Eq. (13) into Eq. (14) further indicates that both z and r depend not only on the vapor pressure P , but also on the pore radius R . As pointed out in Ref. [34], capillary condensation occurs when Eqs. (13) and (14) fail to give a *real* solution for r or z , and this occurs when the LHS of Eq. (14) reaches a minimum. The reason is that the LHS of Eq. (14) is always greater than zero but the RHS falls to zero when $P \rightarrow P_0$. Since the LHS diverges at $z=0$ and $z=R$, it must have a minimum between these limits, and the film thickness can grow from $z=0$ only up to the

point at which this minimum is reached. Thus the threshold thickness (z_c) or radius (r_c) for condensation can be found by minimizing the LHS with respect to either z or r , which gives

$$r_c = (2\gamma/3\alpha)^{1/2} z_c^2. \quad (15)$$

This result shows that even though the *minimum* radius of curvature r increases with the film thickness z , the proportionality between the two lengths is not necessarily linear.

Modeling the fractal surface as a power-law distribution of spherical pores allows us to identify another problem in using Eq. (6) or Eq. (8). From Eqs. (13)–(15), we can determine a threshold pore radius R_c for a given pressure $P < P_0$, such that pores with smaller radii are completely filled and those with larger radii are covered with a film on the surface. The total amount adsorbed at the given pressure is given by

$$N = \frac{4\pi}{3} n \left\{ \int_{R_-}^{R_c} R^3 g(R) dR + \int_{R_c}^{R_+} (R^3 - r^3) g(R) dR \right\}, \quad (16)$$

where R_- and R_+ are the upper and lower limits of the power-law distribution function $g(R)$ and the pressure dependence is implicit in R_c and r . We note that in Yin's derivation [20] of Eq. (6), the film contribution is ignored. This

approximation may be justified theoretically in the limit that the film thickness is much smaller than the pore radius. In practice, however, we can see from Table II that the ratio $V_{\text{full}}/V_{\text{in}}$ is not very large (less than 20). Hence the film in the unfilled pores contains a significant amount of adsorbate that increases with pressure. Qualitatively, separating this amount from the data in Fig. 5 (or Fig. 7) would result in smaller slopes in the log-log plots and give larger D values. To account for this amount quantitatively is difficult, but it would be useful to analyze its effects using the simple model of spherical pores. This will allow us to examine the relative importance of the two terms in Eq. (16).

In summary, we have carried out a detailed adsorption isotherm study on shale samples with known fractal dimensions. We find that fitting the data to the existing theories gives fractal dimensions that are consistently lower than the values determined by SANS. We have discussed several effects that may have caused the discrepancy. We are currently pursuing a numerical study to investigate these effects.

ACKNOWLEDGMENTS

We are grateful to R. A. Guyer and J. Machta for helpful discussions. This work was supported by The Petroleum Research Fund under Grant Nos. 32191-AC2-SF98 and 33549-B9, and the NSF under Grant Nos. DMR-9404672 and CTS-9803387.

-
- [1] See, e.g., W. A. Steele, *The Interaction of Gases with Solid Surfaces* (Pergamon, Oxford, 1974); A. W. Adamson and A. P. Gast, *Physical Chemistry of Surfaces*, 6th ed. (Wiley, New York, 1997).
- [2] S. J. Gregg and K. S. W. Sing, *Adsorption, Surface Area and Porosity* (Academic, New York, 1982).
- [3] P. Pfeifer and D. Avnir, *J. Chem. Phys.* **79**, 3558 (1983); D. Avnir, D. Frain, and P. Pfeifer, *Nature (London)* **308**, 261 (1984).
- [4] A. J. Katz and A. H. Thompson, *Phys. Rev. Lett.* **54**, 1325 (1985).
- [5] H. D. Bale and P. W. Schmidt, *Phys. Rev. Lett.* **53**, 596 (1984).
- [6] P.-Z. Wong, J. Howard, and J.-S. Lin, *Phys. Rev. Lett.* **57**, 637 (1986).
- [7] B. B. Mandelbrot, *The Fractal Geometry of Nature* (Freeman, San Francisco, 1982).
- [8] See, e.g., P. Pfeifer and M. W. Cole, *New J. Chem.* **14**, 221 (1990).
- [9] See, e.g., P. G. de Gennes, in *Physics and Chemistry of Disordered Materials*, edited by D. Alder, H. Fritsche, and S. R. Ovshinsky (Plenum, New York, 1985), p. 227.
- [10] A. V. Neimark, *Russ. J. Phys. Chem.* **64**, 1397 (1990).
- [11] J. M. Drake, P. Levitz, and J. Klafter, *New J. Chem.* **17**, 77 (1990).
- [12] J. J. Fripiat, L. Gatineau, and H. Van Damme, *Langmuir* **2**, 562 (1986).
- [13] M. W. Cole, N. S. Holter, and P. Pfeifer, *Phys. Rev. B* **33**, 8806 (1986).
- [14] S. B. Ross, D. M. Smith, A. J. Hurd, and D. W. Schaefer, *Langmuir* **4**, 977 (1988).
- [15] P. Pfeifer, Y. J. Wu, M. W. Cole, and J. Krim, *Phys. Rev. Lett.* **62**, 1997 (1989).
- [16] B. Sahouli, S. Blacher, and F. Brouers, *Langmuir* **13**, 4391 (1997).
- [17] I. M. K. Ismail and P. Pfeifer, *Langmuir* **10**, 1532 (1994).
- [18] M. Kardar and J. O. Indekeu, *Phys. Rev. Lett.* **65**, 662 (1990).
- [19] D. Avnir and M. Jaroniec, *Langmuir* **5**, 1431 (1989).
- [20] Y. Yin, *Langmuir* **7**, 216 (1991).
- [21] A. V. Neimark, *JETP Lett.* **51**, 607 (1990).
- [22] B. Sahouli, S. Blacher, and F. Brouers, *Langmuir* **12**, 2872 (1996); S. Blacher, R. Pirard, J. P. Pirard, B. Sahouli, and F. Brouers, *ibid.* **13**, 1145 (1997).
- [23] A. V. Neimark, E. Robens, K. K. Unger, and Yu. M. Volkovich, *Fractals* **2**, 45 (1994); A. V. Neimark and K. K. Unger, *J. Colloid Interface Sci.* **158**, 412 (1993).
- [24] H. Darmstadt, C. Roy, S. Kallaguine, B. Sahouli, S. Blacher, R. Pirard, and F. Brouers, *Rubber Chem. Technol.* **68**, 330 (1995).
- [25] B. Sahouli, S. Blacher, F. Brouers, R. Sobry, G. Van Den Bossche, B. Diez, H. Darmstadt, C. Roy, and S. Kallaguine, *Carbon* **34**, 633 (1996).
- [26] D. Rojanski, D. Huppert, H. D. Hale, X. Dacai, P. W. Schmidt, D. Farin, A. Seri-Levy, and D. Avnir, *Phys. Rev. Lett.* **56**, 2505 (1986).
- [27] P.-Z. Wong and A. J. Bray, *Phys. Rev. Lett.* **60**, 1344 (1988).
- [28] A. J. Hurd, D. W. Schaefer, D. M. Smith, S. B. Ross, A. Le Mehaute, and S. Spooner, *Phys. Rev. B* **39**, 9742 (1989).
- [29] M. Jaroniec, *Langmuir* **11**, 2317 (1995).

- [30] See, e.g., G. R. Olhoeft and G. R. Johnson, in *Practical Handbook of Physical Properties of Rocks and Minerals*, edited by R. S. Carmichael (CRC, Boca Raton, FL, 1989).
- [31] We note that although nitrogen molecules are nonspherical, with a *length* of 4.34 Å and a *width* of 3.39 Å, they appear to adsorb with random orientations on heterogeneous surfaces (like molecules in a liquid film) at temperatures above the bulk triple point (~ 63 K). In fact, it has been shown experimentally that the effective area of nitrogen molecules is nearly constant ($\sigma_m = 16.2 \text{ \AA}^2$) on a variety of surfaces at 77 K, which is consistent with the value calculated from the liquid density of nitrogen at 77 K (0.81 g/cm^3) according to Eq. (2.27) in Ref. [2]. For this reason, we use the liquid density at 65 K (0.86 g/cm^3) to obtain the molecular area $\sigma_m \approx 15.6 \text{ \AA}^2$ at the same temperature. See also T. A. Scott, *Phys. Rep.* **27**, 89 (1976).
- [32] See, e.g., *CRC Handbook of Physics and Chemistry*, 58th ed., edited by R. C. Weast (CRC, West Palm Beach, FL, 1977).
- [33] See, e.g., J. H. Page, J. Liu, B. Abeles, H. W. Deckman, and D. A. Weitz, *Phys. Rev. Lett.* **71**, 1216 (1993); T. Shaw, *ibid.* **59**, 1671 (1987)
- [34] S. M. Cohen, R. A. Guyer, and J. Machta, *Phys. Rev. B* **33**, 4664 (1986).